

RESEARCH



Performance assessment of the maximum likelihood ensemble filter and the ensemble Kalman filters for nonlinear problems

Yijun Wang^{1*}, Milija Zupanski², Xuemin Tu³ and Xinfeng Gao¹

*Correspondence: yijun.wang@rams.colostate.edu; wyj1990@rams.colostate.edu ¹Computational Fluid Dynamics and Propulsion Laboratory, Colorado State University, Fort Collins 80523, CO, USA Full list of author information is available at the end of the article Milija Zupanski, Xuemin Tu and Xinfeng Gao these authors contributed equally to this work.

Abstract

This study presents a thorough investigation of the performance comparison of three ensemble data assimilation (DA) methods, including the maximum likelihood ensemble filter (MLEF), the ensemble Kalman filter (EnKF), and the iterative EnKF (IEnKF), with respect to solution accuracy and computational efficiency for nonlinear problems. The convection-diffusion-reaction (CDR) problem is first tested, and then, the chaotic Lorenz 96 model is solved. Both linear and nonlinear observation operators are considered. The study demonstrates that MLEF consistently produces more accurate and efficient solution than the other two methods and provides more information on both states and their uncertainties. The IEnKF and MLEF are used to estimate model parameters and uncertainty in initial conditions using a nonlinear observation operator. The assimilation performance is assessed based on the quality metrics, such as the squared true error, the trace of the error covariance matrix, and the root-mean-square (RMS) error. Based on these DA performance assessments, MLEF demonstrates better convergence and higher accuracy. Results of the CDR problem show significant improvements in the estimate of model parameters and the solution accuracy by MLEF compared to the EnKF family. This study provides evidence supporting the choice of MLEF when solving large nonlinear problems.

Keywords: Data assimilation, Maximum likelihood ensemble filter, Ensemble Kalman filter, CFD Modeling with data assimilation, Ensemble data assimilation methods

1 Introduction

Data assimilation has been playing an indispensable role in the fields of atmospheric science and meteorology for successful weather and climate predictions (e.g., [6,16,30–34]) over the past 50 years. Only recently data assimilation has been brought into the field of engineering (e.g., [7–11,35,36,38,39]) for improving the predictions of computational fluid dynamics (CFD). A brief overview of recent works that are particularly focused on DA applications to flow, turbulence, and combustion demonstrates the effective use of the family of the ensemble Kalman filter (EnKF) (e.g., [8–11,35,36]). Gao and Wang [8–



11,35,36] applied the ensemble Kalman filter (EnKF) to improve the estimate of model parameters for freely propagating laminar flames and investigated issues with the filter divergence. Iterative EnKF (IEnKF) was used in Xiao et al. [41] to treat the nonlinear applications. Labahn et al. [18] employed the EnKF method to examine local extinction events in a jet flame with high-speed measurements. Hurst and Gao [14] applied the ensemble transform Kalman filter (ETKF) with bred vectors to the Kuramoto–Sivashinsky equation to increase the finite limit of the predictability of CFD simulations of chaos. Recently, Wang et al. [38,39] used the maximum likelihood ensemble filter (MLEF) to improve the uncertainty reduction in initial conditions for the time-evolving shear-layer mixing with methane-air combustion and the turbulent flow over a bluff-body geometry. While nonlinear problems are common in engineering, one of the main questions of DA applications is how a DA method is appropriately chosen and assessed. The present work is focused on studying the DA performance for nonlinear problems.

The objective of the present study is to gain a more fundamental understanding of the ensemble filter methods by examining and comparing the applicability and capability of three DA methods—the MLEF [44], the EnKF [6], and the IEnKF [22]. The outcome of the investigation is expected to provide some insights on the DA performance assessment and guidance toward applications of the MLEF and EnKFs methods to the fluid dynamics problem in engineering.

To facilitate understanding of the present work, a brief overview of the necessary background on data assimilation is provided immediately, focusing on the classification of DA methods and their characteristics. More specifically, the similarities and distinctions between the MLEF and EnKFs are delineated at the concept, mathematical formulation, and numerical algorithm levels.

1.1 Data assimilation

Practical DA methods can be broadly categorized into variational and ensemble approaches, along with various hybrid approaches that combine the variational and ensemble methods. Variational DA method (e.g., [2,19]), such as three-dimensional variational (3D-Var) and four-dimensional variational (4D-Var), utilizes optimal control theory to find the analysis state that minimizes a cost function, which is a quadratic function attempting to balance the model prediction and the data. In contrast to the variational method, the ensemble DA method (e.g., [1,4,5,13,40,44,45]) is based on statistical estimation and from the Bayesian point of view, striving to obtain the information about the mean and the covariance of the posterior probability density function (PDF) conditioned on the data. In practice, it is infeasible to determine the complete information, and instead, statistical parameters, such as the mean and/or the variance of the distribution, are sought.

Regardless of classification, all DA methods can, in principle, involve two different types of correction processes: filtering and smoothing. Both processes use observations from the past up to the current time to achieve an optimal state estimate. In filtering, the optimal analysis is achieved by directly estimating the state at the current time, while in smoothing, the state at some moment in the past is changed/optimized, which is then used to predict the state up to the current time. Mathematically speaking, in the analysis step, the filtering process only involves the observation operator, but the smoothing process involves both the prediction model and observation operators.

The core operation of data assimilation is the computation of the forecast error covariance matrices used in the analysis step. Over the years in atmospheric and meteorological research, many types of variational and ensemble DA methods, along with their hybrids, have been developed and applied with the aim of improving the computational efficiency of this operation. Further details can be found in work by Bannister [2], which provides a thorough review of these methods, including their developments, performances, strengths, and limitations. Since ensemble DA methods, in general, are more advantageous than variational methods due to estimating the flow-dependent forecast uncertainty, we focus on understanding the ensemble filters in the present study.

Another important aspect of data assimilation is its ability to address nonlinearity in practical engineering applications. A practical approach to handle the nonlinearity in data assimilation is to apply nonlinear optimization such as gradient-based unconstrained minimization algorithms. Numerical optimization has been a major component of variational data assimilation for decades (e.g., [20,24,27,28,43]) and was later applied to ensemble data assimilation (e.g., [44,45]) and hybrid variational-ensemble DA methods (e.g., [17,37]). It is well-known that one can iteratively use the Kalman filter equations to form a Gauss-Newton minimization algorithm [3]. Alternative ways to address the nonlinearity in the ensemble Kalman filters have been developed as IEnKF methods (e.g., [22,29,42]). These IEnKF often combine empirical arguments with particular numerical optimization algorithms, such as Newton and Gaussian-Newton methods.

In summary, we select three ensemble DA methods—the MLEF, EnKF, and IEnKF methods. Their performance is assessed by focusing on their capabilities to address (i) the nonlinearity of the observation operator and (ii) the chaotic dynamics and the practical physics processes, involving convection, diffusion, and source. The organization of this paper is as follows. Section 2 describes and compares the differences in the mathematical formulations and numerical algorithms among the three ensemble DA methods. The quality measures of DA performance are introduced in Sect. 3. The computational configurations of two model problems and data assimilation are presented in Sect. 4. Results are discussed in Sect. 5. Conclusions are drawn in Sect. 6.

2 MLEF, EnKF, and IEnKF

The MLEF, EnKF, and IEnKF methods follow the main idea of the Kalman Filter (KF); that is that the forecast state and forecast uncertainty are obtained by transporting the analysis and analysis uncertainty through a simulation model (aka forward model). In the EnKF method, the observation operator is linear. The Kalman filter equation is used in the linear update process for solving the optimized state. To address the nonlinearity of the observation operator, IEnKF uses the augmented state approach and iteratively utilizes the Kalman filter equation for optimization. Unlike the EnKF and IEnKF, MLEF does not apply linearization to observation operator during the update process. The forecast state is obtained by conducting a simulation from the current analysis time to the next analysis time, using the current analysis state as the initial conditions for the next DA cycle. To transport uncertainties, one needs to define the initial state for each member in the ensemble as the analysis perturbed by a column of square-root forecast error covariance, which makes MLEF suitable for high-dimensional applications [38,39]. MLEF has a theoretical advantage in nonlinear DA problems over standard ensemble methods and

Table 1 Summary of mathematical notations and symbols used in our DA+CFD system

Notations/symbols	Definition	
U	Vector for solution variables	
α	Vector for model parameters	
$\hat{\mathbf{Q}}$ (used in the MLEF)	Control vector consisting of ${f U}$ and ${f lpha}$	
${f Q}$ (used in the EnKF and IEnKF)	Control variable matrix with all members	
$ar{\mathbf{Q}}$ (used in EnKF and IEnKF)	Ensemble mean vector	
O	Synthesized observation vector	
P	Error covariance matrix w.r.t $ar{\mathbf{Q}}$ or $\hat{\mathbf{Q}}$	
\mathbf{R}	Error covariance matrix w.r.t O	
$\mathcal{M}(\cdot), \mathcal{H}(\cdot)$	Forward model and observation mapping operators	
K	Kalman gain matrix	
Superscript t , f and a	Truth, forecast and analysis state, respectively	
N_e , N_s and $N_{\rm obs}$	The number of ensembles, model states and observations, respectively	

updating error covariance over standard variational methods. It does not need any adjoint calculations. Instead, it uses Hessian as a preconditioner to accelerate the convergence for finding the maximum a posteriori (MAP) point. What follows next is a comparison between the differences in their mathematical formulations and numerical algorithms.

2.1 Difference in the mathematical formulations

For convenience, a list of the consistent mathematical notation and symbols is provided in Table 1, although they are also defined in the text prior to their use.

2.1.1 Ensemble Kalman filter

We select the ensemble Kalman filter (EnKF) developed by Evensen [6]. The solution procedures are described in the following. The forecast state is obtained by conducting a CFD simulation from the current analysis time to the next analysis time when the observation is available, using the current analysis state as the initial condition for the forward model. As an example, to transport uncertainties, the CFD model advances each analysis member, $\mathbf{Q}_{h-1,i}^a$ (i.e., the *i*th column of \mathbf{Q}_{h-1}^a matrix), for getting the forecast state at the *h*th DA cycle as shown by

$$\mathbf{Q}_{h,1}^{f} = \mathcal{M}(\mathbf{Q}_{h-1,1}^{a}),$$

$$\dots$$

$$\mathbf{Q}_{h,i}^{f} = \mathcal{M}(\mathbf{Q}_{h-1,i}^{a}),$$

$$\dots$$

$$\mathbf{Q}_{h,N_{e}}^{f} = \mathcal{M}(\mathbf{Q}_{h-1,N_{e}}^{a}).$$
(1)

where $\mathcal{M}(\cdot)$ is defined as the forward CFD model operator. The superscripts f and a denote the forecast and analysis state, respectively. At the forecast stage, the forecast ensemble mean $(\tilde{\mathbf{Q}}^f)$ and forecast error covariance (\mathbf{P}^f) can be calculated in the form of

$$\tilde{\mathbf{Q}}^f = \frac{1}{N_e} \sum_{i=1}^{N_e} \mathbf{Q}_i^f, \tag{2}$$

The symbol T stands for the transpose. Then, each member in the ensemble is updated at the analysis step with the perturbed observations as

$$\mathbf{Q}_{i}^{a} = \mathbf{Q}_{i}^{f} + \mathbf{K} \left(\mathbf{O}_{i} - \mathbf{H} \mathbf{Q}_{i}^{f} \right), \tag{4}$$

where the Kalman gain matrix is given by

$$\mathbf{K} = \mathbf{P}^f \mathbf{H}^{\mathrm{T}} \left(\mathbf{H} \mathbf{P}^f \mathbf{H}^{\mathrm{T}} + \mathbf{R} \right)^{-1}. \tag{5}$$

H is the linearized observation operator of $\mathcal{H}(\cdot)$ at the forecast mean $(\tilde{\mathbf{Q}}^f)$. The observations, \mathbf{O}_i , are synthesized from the truth (\mathbf{Q}^t) by the following equations,

$$\mathbf{O}_{i} = \bar{\mathbf{O}} + \boldsymbol{\epsilon}_{i}, \quad \bar{\mathbf{O}} = \mathcal{H}\left(\mathbf{Q}^{t}\right) + \boldsymbol{\lambda}, \tag{6}$$

$$\lambda, \epsilon_i \in N(0, \mathbf{R}), \quad i = 1, \dots, N_e.$$
 (7)

Finally, the analysis covariance matrix \mathbf{P}^a can be calculated by

$$\mathbf{P}^{a} = (\mathbf{I} - \mathbf{K}\mathbf{H}) \, \mathbf{P}^{f}, \tag{8}$$

and the subsequent forecast is applied for running to the next DA cycle,

$$\mathbf{Q}_{h+1,i}^{f} = \mathcal{M}_{h}\left(\mathbf{Q}_{h,i}^{a}\right), \quad i = 1, \dots, N_{e}. \tag{9}$$

2.1.2 Iterative ensemble Kalman filter

The Kalman gain matrix in Eq. (5) applies a linear update of the ensemble by linearizing observational operator. However, this linear update process could be problematic when the observational model is strongly nonlinear since the information in the observation data (e.g., experimental measurements) is not fully utilized during the analysis step. As described in work by Lorentzen et al. [22], this can lead to estimates that are not as accurate as they could be. In this work, we adopt the iterative ensemble Kalman filter (IEnKF) method developed by Lorentzen et al. [22]. It does not need any adjoint calculations. It addresses the nonlinearity by introducing an inner-loop iterative process when solving Eq. (4) at the analysis step. Specifically, we show the concept of the inner-loop iterative solver to distinguish the difference from the EnKF method in the following. The threshold of the tolerance (ζ_{tol}) and maximum iteration integer (n) are set to be 0.02 and 12 in the present work, respectively. At an iteration k,

- 1. If k = 0, then we initialize \mathbf{Q}_k and $\tilde{\mathbf{Q}}_k$ as follows
 - · Set each member with

$$\mathbf{Q}_k^i = \mathbf{Q}_h^{f,i}, \quad i = 1, \dots, N_e. \tag{10}$$

· Calculate the mean estimation in the form of

$$\tilde{\mathbf{Q}}_{k} = \frac{1}{N_{e}} \sum_{i=1}^{N_{e}} \mathbf{Q}_{k}^{i}. \tag{11}$$

- 2. Otherwise, we perform the augmented state approach as follows
 - Estimate \mathbf{P}_{k}^{f} based on $\tilde{\mathbf{Q}}_{k-1}$ and \mathbf{Q}_{k-1} by using Eq. (3).
 - Set

$$\mathbf{H}_{k} = \frac{d(\mathcal{H}(\mathbf{Q}))}{d\mathbf{Q}} \bigg|_{\mathbf{Q} = \tilde{\mathbf{Q}}_{k-1}}.$$
(12)

- Evaluate \mathbf{K}_k by using Eq. (5).
- Calculate $(\mathbf{O} \mathbf{H}\mathbf{Q}_k)_i$ for $i = 1, ..., N_e$.
- Update each member, $\mathbf{Q}_k^{1:N_e}$, by using Eq. (4).
- Calculate the mean estimation, $\bar{\mathbf{Q}}_k$, by using Eq. (2).
- Evaluate the L2-norm of the ensemble mean difference by

$$\zeta_k = \sqrt{\frac{\sum_{j=1}^{N_s} (\bar{\mathbf{Q}}_{k,j} - \bar{\mathbf{Q}}_{k-1,j})^2}{N_s}}.$$
(13)

- · Check the following conditions
 - (a) if $\zeta_k \leq \zeta_{\text{tol}}$ or k > n, the augmented state vector, $\tilde{\mathbf{Q}}_k$, is obtained. Then, exit the loop.
 - (b) otherwise, set k = k + 1 and repeat the above steps.

Once exiting from the inner-loop iterative solver, the analysis solution can be updated by

$$\mathbf{Q}_{h}^{a,\{i\}} = \mathbf{Q}_{k}^{\{i\}}, \quad i = 1, ..., N_{e},$$

and then used to reinitialize the next forecast step.

2.1.3 Maximum likelihood ensemble filter

The MLEF method developed by Zupanski [44] is considered. The MLEF method follows the main idea of the Kalman filter (KF), in which the forecast state and the forecast uncertainty are obtained by transporting the analysis and the analysis uncertainty through a simulation model. A cost function is defined and minimized for $\hat{\mathbf{Q}}$ which is a control vector consisting of a vector for the solution variables and a vector for the model parameters. The general derivation of the cost function is based on the Bayes formula, which finds the posterior PDF from the prior, the conditional, and the observation PDFs under Gaussian assumption [15,21]. The cost function is defined as a negative logarithm of the posterior PDF and takes the form of

$$J(\hat{\mathbf{Q}}) = \frac{1}{2} [\hat{\mathbf{Q}} - \hat{\mathbf{Q}}^f]^{\mathrm{T}} \mathbf{P}_f^{-1} [\hat{\mathbf{Q}} - \hat{\mathbf{Q}}^f] + \frac{1}{2} [\mathbf{O} - \mathcal{H}(\hat{\mathbf{Q}})]^{\mathrm{T}} \mathbf{R}^{-1} [\mathbf{O} - \mathcal{H}(\hat{\mathbf{Q}})], \tag{14}$$

where \mathbf{P}_f is the forecast error covariance, \mathbf{R} is the observation error covariance, \mathbf{O} is the observation vector, and $\mathcal{H}(\cdot)$ is again the observation operator mapping the state space to the observation space.

For the forecast state, it can be obtained by conducting a CFD simulation from the current analysis time to the next analysis time, using the current analysis state as the initial condition. Similar to the EnKF method, we define the initial state for each member using the analysis control vector $(\hat{\mathbf{Q}}^a)$ perturbed by a column of square-root error covariance $\mathbf{P}_a^{1/2}$. To transport uncertainties, the CFD model advances the deterministic state $(\hat{\mathbf{Q}}^f)$ and the ensemble forecast (\mathbf{Q}^f) using $\mathbf{P}_{a,i}^{1/2}$ (i.e., the i^{th} column of $\mathbf{P}_a^{1/2}$) at the hth DA cycle as

$$\hat{\mathbf{Q}}_{h}^{f} = \mathcal{M}\left(\hat{\mathbf{Q}}_{h-1}^{a}\right),$$

$$\mathbf{Q}_{h,1}^{f} = \mathcal{M}\left(\hat{\mathbf{Q}}_{h-1}^{a} + \mathbf{P}_{a,1}^{1/2}\right),$$

$$\dots$$

$$\mathbf{Q}_{h,N_{e}}^{f} = \mathcal{M}\left(\hat{\mathbf{Q}}_{h-1}^{a} + \mathbf{P}_{a,N_{e}}^{1/2}\right).$$
(15)

Since the state vector $\hat{\mathbf{Q}}$ is generally multivariate, it can include variables with different orders of magnitude. It is not feasible to invert the forecast error covariance in high-dimensional problems. During the update process, the MLEF algorithm introduces the variable change in the cost function and the minimization process for computational efficiency. For convenience and completeness, the implementation of the variable change and minimization that are used in our previous study [39] is briefly described here. A typical change of variable is applied as

$$\hat{\mathbf{Q}} = \hat{\mathbf{Q}}^f + \mathbf{P}_f^{1/2} \psi. \tag{16}$$

The new control variable ψ is dimensionless. Correspondingly, the cost function (Eq. (14)) is reformulated based on ψ as

$$J(\boldsymbol{\psi}) = \frac{1}{2} \boldsymbol{\psi}^{\mathrm{T}} \boldsymbol{\psi} + \frac{1}{2} \left[\mathbf{O} - \mathcal{H}(\hat{\mathbf{Q}}^f + \mathbf{P}_f^{1/2} \boldsymbol{\psi}) \right]^{\mathrm{T}} \mathbf{R}^{-1} \left[\mathbf{O} - \mathcal{H}(\hat{\mathbf{Q}}^f + \mathbf{P}_f^{1/2} \boldsymbol{\psi}) \right]. \tag{17}$$

However, Eq. (17) is not the final form to be solved because the system is stiff, which can be indicated by the condition number of the Hessian matrix, $\nabla^2 J(\psi)$. To achieve a fast convergence of minimization and a good estimate of analysis error covariance in the system, another change of variable is introduced, referred to as the Hessian preconditioning

$$\psi = \left[\mathbf{I} + \left(\mathbf{Z}(\hat{\mathbf{Q}})\right)^{\mathrm{T}} \left(\mathbf{Z}(\hat{\mathbf{Q}})\right)\right]^{-1/2} \xi,\tag{18}$$

where ξ is the final control variable, and $\mathbf{Z}(\hat{\mathbf{Q}})$ is a $N_{\mathrm{obs}} \times N_e$ matrix defined with $[\mathbf{z}_1, \mathbf{z}_2, \dots, \mathbf{z}_{N_e}]$ as

$$\mathbf{z}_{i} = \mathbf{R}^{-1/2} \left[\mathcal{H}(\hat{\mathbf{Q}} + \mathbf{P}_{f,i}^{1/2}) - \mathcal{H}(\hat{\mathbf{Q}}) \right], \quad i = 1, 2, \dots, N_{e},$$
 (19)

where $N_{\rm obs}$ is the number of available observation data. The Hessian preconditioning significantly reduces the condition number, which helps speed up the convergence rate of the iterative minimization methods. In the process of minimization, both the first

derivative and second derivative with respect to ξ are required. The iterative update of the control variable ξ is

$$\boldsymbol{\xi}_{k+1} = \boldsymbol{\xi}_k + \alpha_k \mathbf{d}_k,\tag{20}$$

where k is the minimization iteration index, \mathbf{d} is the descent direction vector, and α is the step length. The calculations of α and descent direction depend on the minimization algorithm used. A few minimization methods have been experimented with and discussed in our previous work [39]. For example, the simplest one is the steepest descent method [12]. It only relies on the information of the local gradient of the cost function for the direction of finding the optimal solution. Its performance is poor in terms of the convergence rate. The quasi-Newton method [23] determines the optimal direction based on the Hessian matrix by storing the information of the local curvature of the cost function. It converges much faster than the steepest descent method. In this work, we use the quasi-Newton method. During the minimization process, the initial step-length is $\alpha=1$, and the optimal α is determined to satisfy the Wolfe conditions in each iteration (Chapters 8 and 10 in Nocedal and Wright [26]). Then, the \mathbf{d}_k is updated by

$$\mathbf{d}_k = -\mathbf{S}_k \nabla_{\xi} J(\hat{\mathbf{Q}}_k),\tag{21}$$

where S_k is defined as the inverse Hessian matrix. At k = 1, it can be calculated as

$$\mathbf{S}_1 = \left(\nabla_{\boldsymbol{\xi}}^2 J(\hat{\mathbf{Q}}_1)\right)^{-1}.\tag{22}$$

For k > 1, S_k can be updated in that form of

$$\mathbf{S}_{k} = \left(\mathbf{I} - \boldsymbol{\lambda}_{k-1} \boldsymbol{\beta}_{k-1} \boldsymbol{\omega}_{k-1}^{\mathrm{T}}\right)^{\mathrm{T}} \mathbf{S}_{k-1} \left(\mathbf{I} - \boldsymbol{\lambda}_{k-1} \boldsymbol{\beta}_{k-1} \boldsymbol{\omega}_{k-1}^{\mathrm{T}}\right) + \boldsymbol{\lambda}_{k-1} \boldsymbol{\omega}_{k-1} \boldsymbol{\omega}_{k-1}^{\mathrm{T}}, \tag{23}$$

where the terms λ_{k-1} , $\boldsymbol{\beta}_{k-1}$ and $\boldsymbol{\omega}_{k-1}$ are given by $\lambda_{k-1} = \nabla_{\boldsymbol{\xi}} J(\hat{\mathbf{Q}}_k) - \nabla_{\boldsymbol{\xi}} J(\hat{\mathbf{Q}}_{k-1})$, $\boldsymbol{\beta}_{k-1} = \alpha_{k-1} \mathbf{d}_{k-1}$, and $\boldsymbol{\omega}_{k-1} = 1/\left(\lambda_{k-1} \boldsymbol{\beta}_{k-1}^{\mathrm{T}}\right)$, respectively. The minimization process starts with the initial guess $\boldsymbol{\xi}_{k=0} = 0$, which means

$$\hat{\mathbf{Q}}_{k=0} = \hat{\mathbf{Q}}^f. \tag{24}$$

After the optimal value of ξ_k is obtained, the analysis deterministic state vector $\hat{\mathbf{Q}}^a$, as the minimizer of Eq. (14), is then calculated by

$$\hat{\mathbf{Q}}^a = \hat{\mathbf{Q}}^f + \mathbf{P}_f^{1/2} \left[\mathbf{I} + \left(\mathbf{Z}(\hat{\mathbf{Q}}^f) \right)^{\mathrm{T}} \left(\mathbf{Z}(\hat{\mathbf{Q}}^f) \right) \right]^{-1/2} \boldsymbol{\xi}_k.$$
 (25)

Then, $\hat{\mathbf{Q}}^a$ is used to update the square-root analysis error covariance,

$$\mathbf{P}_a^{1/2} = \mathbf{P}_f^{1/2} \left[\mathbf{I} + \left(\mathbf{Z}(\hat{\mathbf{Q}}^a) \right)^{\mathrm{T}} \left(\mathbf{Z}(\hat{\mathbf{Q}}^a) \right) \right]^{-1/2}.$$
 (26)

Finally, a Gaussian perturbation to $\hat{\mathbf{Q}}^a$ is made to prepare for each member in the ensemble as initial conditions for the next DA cycle,

$$\mathbf{Q}_{i}^{a} = \hat{\mathbf{Q}}^{a} + \mathbf{P}_{a,i}^{1/2}, \quad i = 1, \dots, N_{e}. \tag{27}$$

where $\mathbf{P}_{ai}^{1/2}$ is the *i*th column in the $\mathbf{P}_{a}^{1/2}$ matrix.

2.2 Difference in the numerical algorithms

All methods involve three major steps: (i) initiation step, (ii) forecast step, and (iii) analysis step. The main difference is in the analysis step. EnKF/IEnKF calculate N_e analyses to obtain the analysis mean, while MLEF calculates only a single analysis. Algorithms 1-3 present the major steps in each component for three ensemble-based DA methods, respectively. In the EnKF and IEnKF methods, observations have to be perturbed when evaluating the observation increments with respect to each member in the ensemble, then the Kalman gain matrix (K) is introduced and used to update each member in that ensemble sequentially by linearizing the observation impact from the observation space into the model state space. As shown in line 18 of Algorithm 1, the EnKF method solves the optimized state by the linear update process using the Kalman filter equation (Eq. 4). Lines 16 and 17 of Algorithm 2 show that the IEnKF method uses the augmented state approach and utilizes Eq. (4) in an iterative manner to form a minimization algorithm on addressing the nonlinearity of the observation operator. In the MLEF method, as presented in lines 20–25 of Algorithm 3, an iterative minimization solver is applied to the cost function (Eq. 14) for the optimization.

IEnKF essentially belongs to the Gauss-Newton (GN) method for nonlinear least squares (e.g., Sakov et al. [29]). However, successful performance of the GN method is limited to small residuals or to residuals being linear functions (see Chapter 10 in Nocedal and Wright [26]). There is a fundamental assumption in GN that approximates the Hessian using Jacobian matrices, which has limited applicability. Although several improvements of GN method have been proposed (e.g., line search, Levenberg-Marquardt method), most often the preferable minimization method is a standard unconstrained minimization, such as nonlinear conjugate-gradient (CG) or quasi-Newton method (QN) (e.g., Nocedal and Wright [26]). MLEF does exactly that; it employs unconstrained minimization with line search (the QN method in the present study). CG and QN methods are more suitable for handling arbitrary nonlinearity than GN method, from both theoretical and practical points of view (see Chapters 5, 8 and 10 in Nocedal and Wright [26]). Because of that it can only be expected that MLEF outperforms IEnKF in majority of situations. A more detailed comparison between the CG/QN and GN methods would have to specifically address the components of the GN algorithm, such as the validity of Hessian approximation and line search. Although potentially beneficial, such comparative study would amount to a new manuscript, and therefore it is left for the future.

In addition, the optimal deterministic state vector is solved in the ensemble space (N_e) in the MLEF method, then it is used to update the analysis error covariance matrix and the members to reinitialize the new DA cycle. However, the potential computational cost of the MLEF method is still comparable to that of the EnKF and IEnKF methods. Based on our experience in lower-dimensional problems ($N_s \leq 10^5$), they are mostly on the same order of magnitude. For high-dimensional problems, covariance localization is a standard feature in ensemble-based DA applications. However, covariance localization is typically used only in severely ill-conditioned problems. To quantify ill-conditioning, a general rule-of-thumb is to estimate the order of magnitude of the ratio between state and ensemble dimensions. When this ratio is equal to several orders of magnitude, then covariance localization is required. For example, in realistic data assimilation problems, one typically employs $O(10^2)$ ensembles for $O(10^7)$ state dimension, making the ratio between the state and ensemble dimensions of the order of $O(10^5)$. For low-dimensional problems considered in this manuscript, the ratio is approximately O(10), which makes the use of localization harder to justify. In addition, covariance localization introduces a set of new empirical parameters for specifying the localization scale. With localization, it is also customary for EnKF to include covariance inflation with its own set of empirical parameters. Therefore, adding covariance localization will likely make this comparison overly dependent on the optimal choice of localization and inflation parameters, as well as on the chosen method for inflation. While this may be necessary for high-dimensional applications, it can unnecessarily contaminate the results of low-dimensional applications presented here.

Algorithm 1 EnKF Method

Step 1: Initialization

```
1: Initial Step (\mathbf{Q}_0^{1:N_e})
2:
        Select the initial conditions of uncertainties.
        if (Uncertainty in model states) then
3:
 4:
            Use the lagged forecast method [16].
5:
        end if
        if (Uncertainty in model parameter) then
 6:
7:
            Use Box–Muller transform method [25].
8.
        end if
        Construct \mathbf{Q}_0^{1:N_e}.
 9.
10: end
```

Step 2: Forecast Step

```
11: Forecast Step (\mathbf{Q}^f, \mathbf{P}^f)

12: Propagate \mathcal{M}(\mathbf{Q}^{1:N_e}) from t_{h-1} to t_h.

13: Calculate \bar{\mathbf{Q}}^f and \mathbf{P}^f by Eq. 2 and 3.

14: end
```

Step 3: Analysis Step

```
15: Analysis Step (\mathbf{Q}^a, \mathbf{P}^a)

16: Calculate (\mathbf{O} - \mathbf{HQ})_i for i = 1, ..., N_e.

17: Evaluate \mathbf{K} by Eq. 5.

18: Update \mathbf{Q}^a by Eq. 4..

19: Calculate \mathbf{P}^a by Eq. 8.

20: end

21: Next DA cycle
```

Algorithm 2 IEnKF Method

Step 1: Initialization

```
1: Initial Step (\mathbf{Q}_0^{1:N_e})
2:
        Select the initial conditions of uncertainties.
        if (Uncertainty in model states) then
3:
            Use the lagged forecast method.
 4:
        end if
5:
 6:
        if (Uncertainty in model parameter) then
7:
            Use Box-Muller transform method.
8:
        Construct \mathbf{Q}_0^{1:N_e}.
9:
10: end
```

Step 2: Forecast Step

```
11: Forecast Step (\mathbf{Q}^f, \mathbf{P}^f)
            Propagate \mathcal{M}(\mathbf{Q}^{1:N_e}) from t_{h-1} to t_h.
12:
            Calculate \mathbf{Q}^f and \mathbf{P}^f by Eq. 2 and 3.
13:
14: end
```

Step 3: Analysis Step

```
Analysis Step (\mathbf{Q}^a, \mathbf{P}^a)
15:
16:
         Call Inner-loop Iterative Solver..
17:
         Update \mathbf{Q}^a with the output from last step..
         Calculate \mathbf{P}^a by Eq. 8.
18:
19: end
20: Next DA cycle
```

3 Performance measures

In order to assess the DA performance, three validation measurements are used—the squared true error diagnostics, the trace of \mathbf{P}^a , and root-mean-square (RMS) error. These measures are prescribed as follows and used for the performance assessment in the results.

The squared true error diagnostics is used in the context of ensemble DA methods. The value can be evaluated by the total difference between the truth and the DA+CFD prediction in the form of

$$\epsilon_t = \left(\mathbf{Q}^t - \tilde{\mathbf{Q}}\right)^{\mathrm{T}} \left(\mathbf{Q}^t - \tilde{\mathbf{Q}}\right),\tag{28}$$

where \mathbf{Q}^t denotes the truth vector and $\tilde{\mathbf{Q}}$ represents the mean predicted solution vector by the data assimilation. Assuming there is no uncertainty in the initial and boundary conditions as well as in the physical models and model parameters, the numerical simulation obtained by the perfect CFD model is regarded as the "truth" in this study. The analysis ensemble mean vector $(\mathbf{\tilde{Q}}^a)$ of the EnKF and IEnKF methods and the analysis deterministic vector (\mathbf{Q}^a) of the MLEF method are used as the mean prediction for this calculation. The expected values for ϵ_t should decrease as more DA cycles are performed.

Algorithm 3 MLEF Method

Step 1: Initialization

```
1: Initial Step(\mathbf{Q}_0^{1:N_e},\hat{\mathbf{Q}}_0)
         Select the initial conditions of uncertainties.
2:
3:
         if (Uncertainty in model states) then
             Use the lagged forecast method.
4:
         end if
5:
 6:
         if (Uncertainty in model parameter) then
7:
             Use Box-Muller transform method.
8:
        Construct \mathbf{Q}_0^{1:N_e} and \hat{\mathbf{Q}}_0.
9:
10: end
```

Step 2: Forecast

```
11: Forecast Step(\mathbf{Q}^f,\mathbf{P}^f)
12: | Propagate \mathcal{M}(\mathbf{Q}^{1:N_e}) and \mathcal{M}(\hat{\mathbf{Q}}) from t_{h-1} to t_h.
13: | Obtain \mathbf{Q}^f and \hat{\mathbf{Q}}^f.
14: | Calculate \mathbf{P}_f^{1/2}.
15: end
```

Step 3: Analysis

```
Analysis Step(\hat{\mathbf{Q}}^a, \mathbf{P}^a)
16:
          Set \hat{\mathbf{Q}}_{k=0} = \hat{\mathbf{Q}}^f.
17:
18:
          Apply change of variable \psi_{k=0}.
19:
          Evaluate the Hessian preconditioner by Eq. 18.
          while 1 \le k \le n do
20:
               Calculate S_k by Eq. 22 or 23.
21:
               Calculate \mathbf{d}_k by Eq. 21.
22:
               Estimate \alpha_k.
23:
               Update \xi_k by Eq. 20.
24:
25:
          end while
          Update \hat{\mathbf{Q}}^a by Eq. 25.
26:
          Calculate \mathbf{P}_a^{1/2} by Eq. 26.
27:
28:
          Update \mathbf{Q}_i^a for i = 1, ..., N_e by Eq. 27.
29: end
30: Continue the next DA cycle.
31: Repeat Steps 1-3.
```

The other important statistical verification of the ensemble filter algorithm is to calculate the trace value of the analysis error covariance matrix, which indicates the filter performance on the uncertainty reduction during the DA process. Since the uncertainty error is expected to be reduced by the available observations, the variance of the members should decrease and converge to a sufficiently small tolerance as more DA cycles are performed. The expected values for $\operatorname{trace}(\mathbf{P}^a)$ should be close to a sufficiently small tolerance as possible.

Finally, the RMS error can be calculated based on the synthesized observation and the predicted solution vector, as

$$RMS_i = \sqrt{\frac{\sum_{j=1}^{N_{obs}} \left(\mathbf{O} - \mathcal{H}(\tilde{\mathbf{Q}})\right)_j^2}{N_{obs}}}.$$
 (29)

Overall, the value of the RMS error is expected to decrease as more DA cycles are performed.

4 Tests and DA configurations

The DA+CFD system is applied to the 1D convection-diffusion-reaction (CDR) problem and the Lorenz 96 model. These problems are chosen because the truth for each problem is available for the performance assessment. More importantly, these problems represent physics of interest to engineering fluids problems. The CFD predictions are compared among the DA analyses using the EnKF, IEnKF, and MLEF methods. The assimilation performance is assessed using the true error diagnostics, the trace of \mathbf{P}^a , and the RMS error as prescribed above.

The present study has been carried out on Atlantis, an internal high-performance compute server managed by the Computational Fluid Dynamics and Propulsion group at Colorado State University. It consists of nine compute nodes and 189 TB of storage connected by a 40 Gbps InfiniBand network. In total, there are 200 cores on the compute nodes.

4.1 The convection-diffusion-reaction Model

The one-dimensional transient inhomogeneous CDR problem from our previous DA study [9,11,35,36] with the EnKF method is used to verify the MLEF method. Assume that the model parameters are inaccurate and need to be estimated by data assimilation. In addition, we are interested in assessing how the adverse impact of imperfect initial conditions on predictions can be removed or mitigated by data assimilation. Specifically, the uncertain model parameters to be estimated are γ , μ , and c in the CDR equation,

$$\frac{\partial \phi}{\partial t} + \gamma \frac{\partial \phi}{\partial x} - \mu \frac{\partial^2 \phi}{\partial x^2} + c\phi = f, \quad 0 \le x \le 1,$$
(30)

where ϕ is the solution variable. For convenience, the true values for the convection speed, γ , the diffusivity, μ , and source term coefficient, c, are known and they are all unity. The other source term, f, is modeled by $f = 2(x-1)e^{-t}$. Dirichlet boundary condition is applied for the inlet, and Neumann boundary condition is specified for the outlet domain extent. The analytical solution of the problem is used as the truth and defined in the form of

$$\phi^t(x,t) = x^2 e^{-t}. ag{31}$$

Three tests are configured. The first case examines the consequence of an imperfect initial condition on the solution field. The second test investigates the situation in which the errors exist in both the initial condition and the three model parameters simultaneously.

The third test focuses on filter performance with a nonlinear quadratic observation operator. The assimilation performance for each case is assessed by comparing the solution differences between the truth and the DA+CFD predictions at the end of the DA cycles.

4.2 The Lorenz 96 model

The Lorenz 1996 model is commonly used as a model problem in data assimilation. The model equation is given by

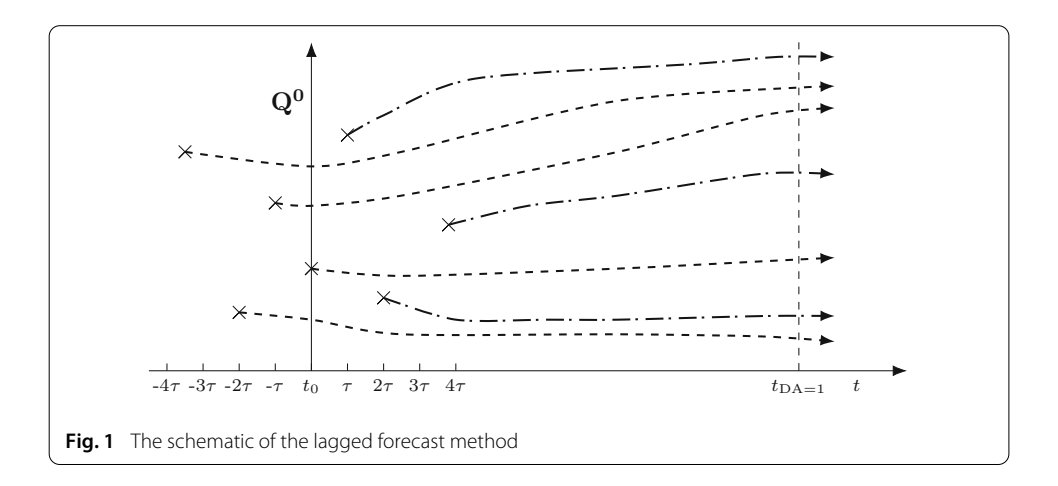
$$\frac{\mathrm{d}x_j}{\mathrm{d}t} = (x_{j+1} - x_{j-2}) x_{j-1} - x_j + F, \quad j = 1, 2, \dots, N_x,$$
(32)

where N_x represents the total number of variables. In this study, we use $N_x=20$. F is the source term for enforcing the system to be a chaotic regime, which has the value of 8.17. A strong positive or negative correlation is observed for each variable with respect to the adjacent variable components in the vector. The periodic boundary condition is applied in the system. The numerical solution is simply obtained by discretizing Eq. (32) in the temporal space using a fourth-order Runge–Kutta time marching scheme with a constant time step $\Delta t=0.001$. The truth of this problem is adopted as the solution that is propagated from the initial condition of setting the first component of the model variable to be 0.1 and the rest of them to be zero.

4.3 Configurations of data assimilation

The main concept of data assimilation is uncertainty error estimation and reduction. In the current modeling system, the observation errors are assumed to be unbiased and followed by the Gaussian distribution along the whole DA process. The conservative variables in the initial condition and the initial model parameters are considered to have uncertainties. However, the discretization errors introduced by the CFD forward model are neglected, which is considered as a "perfect model scenario." In addition, in data assimilation, the observations are normally the experimental measurements in space and time, whose spatial and temporal scales depend on the technique used to make the measurements. Then, since observations are not necessarily the same variables as those solved by the forward model, the choice of the observation operators could have a significant impact on the statistical error analysis. The observations used in the following two cases are synthesized from the perfect model. In addition, for the purpose of getting better performance assessments, a free CFD run (i.e., data assimilation is not applied) is performed to compare the predictions of 3 different DA methods and the truth.

It is worth emphasizing that, before any data assimilation can begin, it is necessary to define an initial state (including solution variables and empirical parameters) and the uncertainty of that initial state. For the initial conditions of data assimilation, we often use the lagged forecast method [16], as illustrated by Fig. 1. That is, given the time for which the initial state and its uncertainty are needed, $t_h=0$, a deterministic simulation of length $4t_{\tau}$ is started from a time $t_h=-2t_{\tau}$ in the past. The time t_{τ} can typically be equal to the assimilation frequency window (T_{DA}). For an ensemble with N_e members, one runs N_e+1 CFD simulations in the MLEF method while N_e in the EnKF family method, which can be equally distributed over the $4T_{DA}$ interval. In this approach, we use time-lagged simulations as members in the ensemble. The initial deterministic state may be set by the simulation whose start is at $t_h=0$, or simply the ensemble mean of N_e members. For the



initial uncertainty of empirical parameters, we use random perturbations, currently based on a Gaussian probability density function. However, the lagged forecast method is not an inherent component of any of these DA methods. It is chosen here because it has a good record in applications to various time-dependent problems in meteorology. When using the lagged forecast method, some spatial differences and the uncertainty correlation between the model variables and the model parameters are included as dynamical features are advected over time. Based on our experience, it can help to reduce the unphysical perturbation noise when forming the initial forecast error covariance matrices in ensemble DA methods, which could benefit these methods to be able to recover more correct error covariance after only a couple of DA cycles.

5 Results and discussion

5.1 Imperfect initial condition in steady-mode problem

We start the investigation of the DA impact on the imperfect initial condition for the one-dimensional transient inhomogeneous CDR model problem, which eventually has a steady-state solution. The computational domain size for the problem is set to be $L_x = 1$ m. Total of 128 cells are used. The DA frequency is set to be every 5000 time steps, and the time step size is $\Delta t = 1 \times 10^{-5}$ s, that is that a DA cycle occurs every 0.05 sec along the propagation of forward model. The sensitivity study of the ensemble size for the CDR problem was performed in our previous study [36], which led to an ensemble consisting of 8 members. We use the same ensemble size in this work. A small amount of perturbations is added into the initial CFD condition for propagating the solution using the lagged forecast method as

$$\phi(x, t = 0) = x^2 \sin\left(\beta_1 \frac{2\pi x}{L_x} + \beta_2\right), \quad \beta_1 \in N(0.1, 0), \quad \beta_2 \in N(0.01, 0).$$
 (33)

The initial members in the ensemble are presented and compared to the truth in Fig. 2. The first case is to assess the assimilation performance and make a comparison among the EnKF, IEnKF, and MLEF methods when the observation operator is linear. The observation operator, $\mathcal{H}(\cdot)$, is given by

$$\mathcal{H}(\phi_j) = \phi_j, \quad j = 1, 2, \dots, N_{\text{obs}}. \tag{34}$$

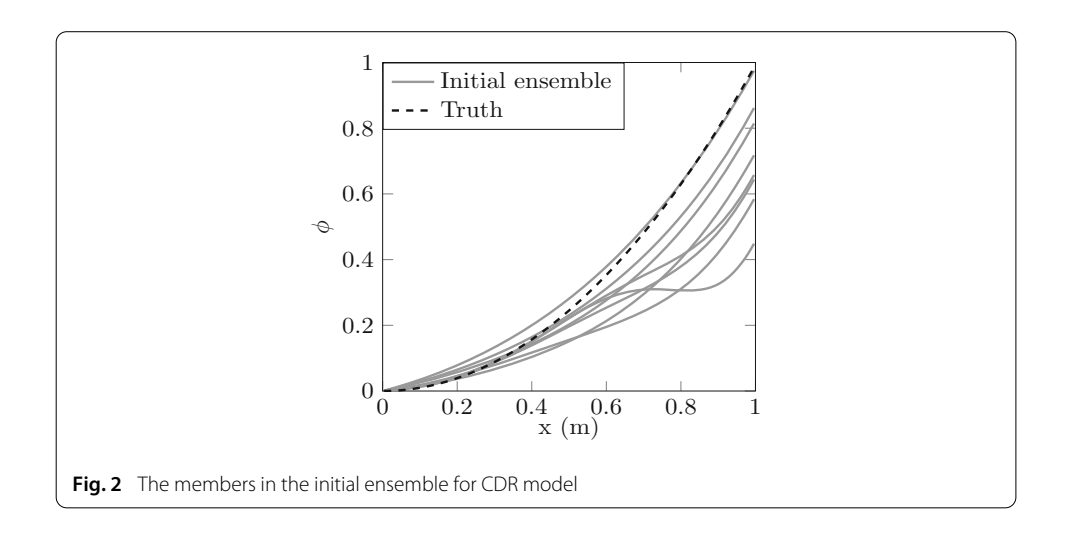


Table 2 DA+CFD configurations for imperfect initial condition in the steady-mode problem (referred as "case 1")

Forward model	Configuration	
Equation	CDR model (see Sect. 4.1)	
Computational domain	$L_x = 1 \mathrm{m}$ with 128 cells	
Time step (Δt)	$1 \times 10^{-5} \mathrm{s}$	
Boundary condition	Inlet: Dirichlet boundary condition	
	Outlet: Neumann boundary condition	
DA	Configuration	
Size of the ensemble	8 (EnKF, IEnKF), 8 + 1 (MLEF)	
Uncertainty	Solution variable (ϕ)	
Initial guess	ϕ : generated by lagged forecast method	
Frequency	5000 time steps	
Synthesized Observation	At every other 4 cells:	
	Linear test: $\mathbf{O} = \phi$.	
	Nonlinear test: $\mathbf{O} = 2.5\phi^2 + 1.5\phi$.	
Observation error	N(0, 0.15)	
Methods	Linear test: EnKF, IEnKF, and MLEF	
	Nonlinear test: IEnKF and MLEF	
Total DA cycle	15 cycles	

The observations are synthesized from the perfect model at every other 4 cells by adding noise with the error distribution N(0,0.15). The DA performance is first assessed by comparing the predictions of each DA method with the truth. The summary of the DA+CFD configuration is shown in Table 2. The results in Fig. 3 show the predictions of each member and their mean estimation in 3 columns and 3 rows. For the MLEF method, we use the prediction of the control vector as its mean estimation. In each column, the predictions from different DA methods are compared to the truth at the same DA cycles. Rows show the comparisons at 5th, 10th, and 15th DA cycles, respectively. At the 5th DA cycle, the variance of the members by the MLEF method is the smallest, which indicates that MLEF has a better convergence rate of uncertainty reduction than the other two methods. In addition, as more DA cycles are performed, all the DA predictions are getting closer toward the truth, which is what we expected from a proper DA process.

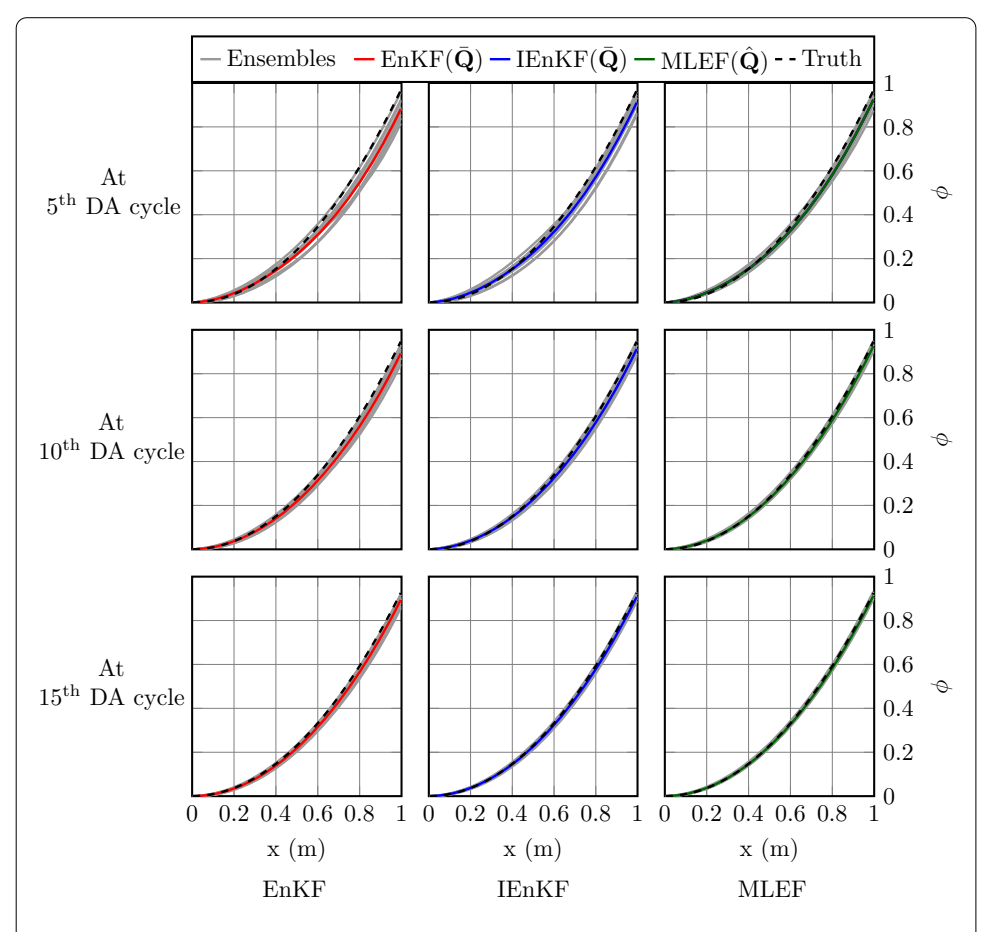


Fig. 3 Solution comparisons among the EnKF (1st column), IEnKF (2nd column), and MLEF (3rd column) methods at the 5th, 10th, and 15th DA cycles for the linear test in case 1

The performance is further assessed by measures of the true error, the trace of P^a matrix, and the RMS error along the DA process. By tracking the trajectories of the convergence history in Fig. 4a-c, we clearly see that the IEnKF method shows faster convergence at the beginning of DA process. But, the MLEF method results in a smoother and higher error reduction rate than both the EnKF and IEnKF methods along the DA process. Moreover, we calculate the absolute solution difference, $\|\Delta\phi\| = \|\phi^{\mathrm{DA}} - \phi^t\|$, over the computational domain after 15 DA cycles. The MLEF prediction shows the smaller difference in the results among the 3 DA methods in Fig. 4d.

Furthermore, we investigate the performance of the MLEF and IEnKF methods for the case of using a nonlinear quadratic observation operator, where $\mathcal{H}(\cdot)$ is given by

$$\mathcal{H}(\phi_j) = 2.5\phi_j^2 + 1.5\phi_j, \quad j = 1, 2, \dots, N_{\text{obs}}.$$
 (35)

The DA setups are the same as those in the previous case; that is the same in the assimilation frequency and the initial ensemble for the initial condition. In this case, the assessment of the performance depends on tracking the convergence histories of the true error, the trace of \mathbf{P}^a matrix, and the RMS error along the DA process. The trajectories for the true error estimation and the trace of P^a matrix are shown in Fig. 5a, b, respectively. Both methods have achieved an error reduction of more than 95% within 6 DA cycles. As the

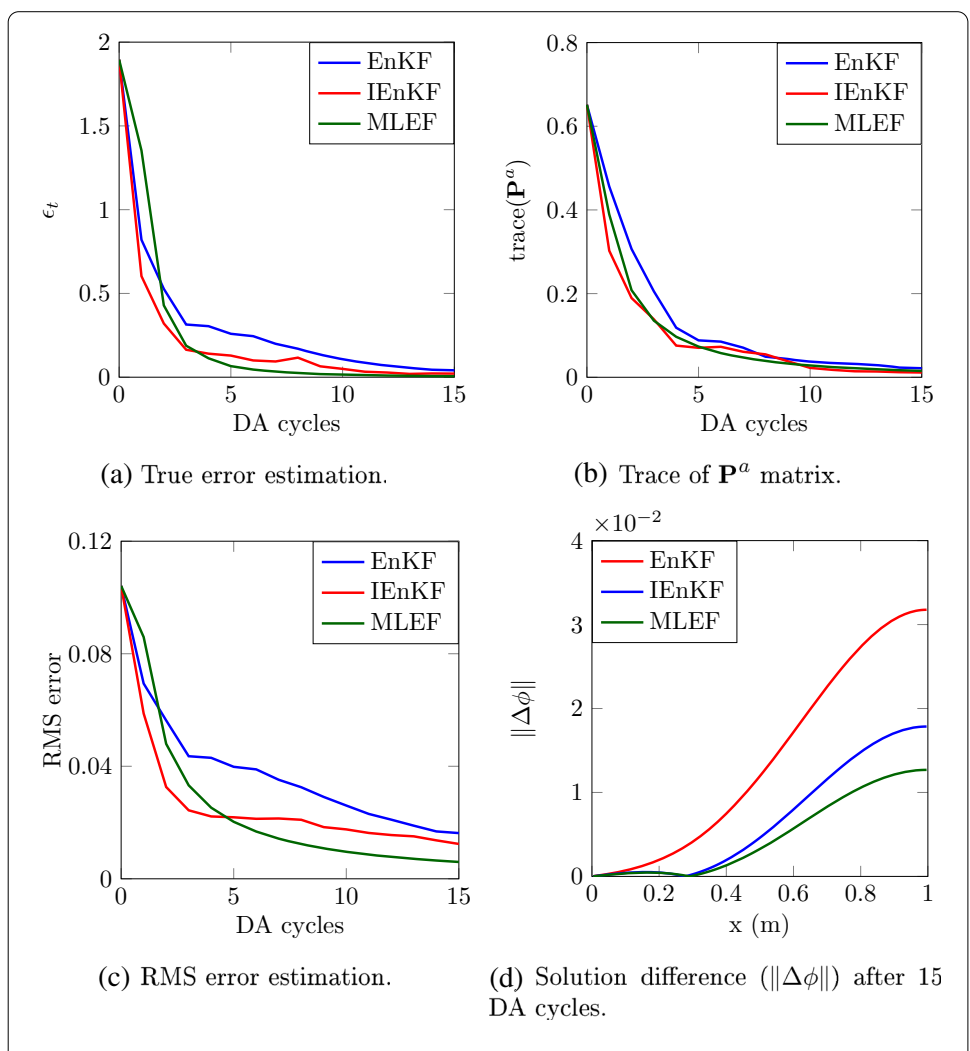


Fig. 4 Comparisons of different measures among the EnKF (blue line), IEnKF (red line), and MLEF (green line) methods for the linear test in case 1

DA predictions converge toward the truth, the overall impact of data assimilation on the CFD simulations decreases as expected. Similarly, the RMS error can be considered for the quality assessment of data assimilation. As shown in Fig. 5c, the MLEF method drives the RMS error down much lower in the case of the quadratic observation operator. The solution differences between the truth and the DA+CFD predictions at the last DA cycle are shown in Fig. 5d. The final prediction by MLEF shows a better convergence toward the truth than IEnKF.

5.2 Errors in both initial condition and multiple parameters

We investigate the performance of the MLEF and IEnKF methods with the same non-linear observation operator for the situation in which the uncertainties exist in both the initial condition and the three model parameters (γ , μ , and c) simultaneously. For each model parameter, members are selected randomly by following a normal distribution. The normal distribution curves used here have the mean value of 3.0 and standard deviation of 1.0 for generating the initial guess of μ and c, and using the mean value of 4.0

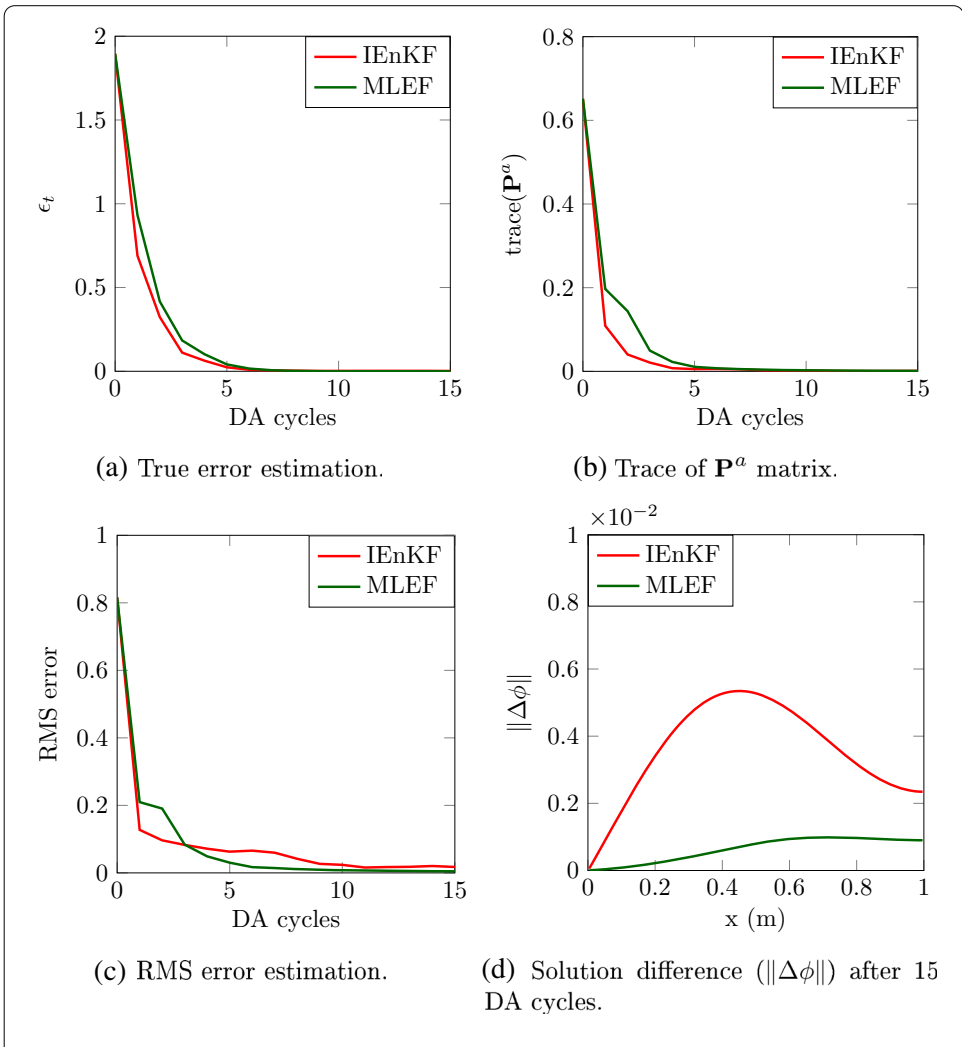


Fig. 5 Comparisons of different measures between the IEnKF (red line) and MLEF (green line) methods for the nonlinear test in case 1

and standard deviation of 2.0 for the initial guess of γ . The DA setups remain the same as those in the above cases. The summary of the DA+CFD configuration for the problem is shown in Table 3. Since the magnitude of the errors in the model parameters and the initial condition are of a different order of magnitude, tracking the overall true error would not be particularly instructive. Instead, we plot the trajectories of the convergence history of the true error estimation for the model parameters and the solution variable separately in Fig. 6a, b. We clearly can see that some fluctuations occur in the results by the IEnKF method, while the results by the MLEF method show nice and smooth convergence history along the DA process. The error takes a much longer time to be adjusted or converged to a lower magnitude for this case. This is not surprising because the model parameters are not observed components in the given observation and can only get corrected through the covariance between the coupled uncertainties with the solution variable. Similar oscillation phenomena are observed in the results of the IEnKF method when tracking the trajectories of the trace value of only the solution variable part of \mathbf{P}^a matrix along the entire DA process in Fig. 6c. Figure 6d compares the final DA predictions

Table 3 DA+CFD configurations for errors in both initial condition and multiple parameters (referred as "case 2")

Forward model	Configuration	
Equation	CDR model (see Sect. 4.1)	
Computational domain	$L_x = 1 \text{ m with } 128 \text{ cells}$	
Time step (Δt)	1×10^{-5} s.	
Boundary condition	Inlet: Dirichlet boundary condition	
	Outlet: Neumann boundary condition	
DA	Configuration	
Size of the ensemble	8 (IEnKF), 8 + 1 (MLEF)	
Uncertainty	Solution variable (ϕ) and 3 model parameters (γ , μ , and	
	<i>c</i>)	
Initial guess	ϕ : generated by lagged forecast method	
	μ and c : generated by Box–Muller transform method	
	with mean of 3.0 and standard deviation of 1.0	
	γ : generated by Box–Muller transform method with	
	mean of 4.0 and standard deviation of 2.0	
Frequency	5000 time steps	
Synthesized observation	At every other 4 cells:	
	Nonlinear test: $\mathbf{O} = 2.5\phi^2 + 1.5\phi$	
Observation error	N(0, 0.15)	
Methods	Nonlinear test: IEnKF and MLEF	
Total DA cycle	40 cycles	

by the IEnKF and MLEF methods to the truth along with the free CFD runs. In addition, the trajectories of each model parameter by the two DA methods are plotted in Fig. 7. Clearly, MLEF efficiently and effectively improves the estimate of the model parameters and the prediction.

5.3 Imperfect Initial Condition in Chaotic-mode Problem

We continue the investigation of the DA impact on the imperfect initial condition of the Lorenz 1996 model (L96) problem. A sensitivity study of the ensemble size is performed first using the IEnKF method for the consideration of both the solution accuracy and computational efficiency. A linear observation operator is applied in the form of

$$\mathcal{H}(X_i) = X_i, \quad j = 1, 2, \dots, N_{\text{obs}}.$$
 (36)

The observations are synthesized from the perfect model at every cell by adding noise with the error distribution N(0,0.5). The initial members are generated by randomly perturbing the initial condition. The DA frequency is set to be every 100 time steps, and the time step is $\Delta t = 0.001$ s. Six ensembles, consisting of 4, 6, 8, 10, 12, and 14 members, respectively, are generated. The total computational costs and the cost increments on average are reported in Table 4 with respect to each ensemble size. The trajectories of the convergence history of the RMS error are plotted in Fig. 8. We find that an ensemble consisting of 12 members shows the best performance in the aspects of both the solution accuracy and computational efficiency along the DA process. In the following test cases, we use 12 members in the ensemble.

The DA performance is first assessed by comparing the solution of the model states between the predictions by the three DA methods and the truth. We use the same linear

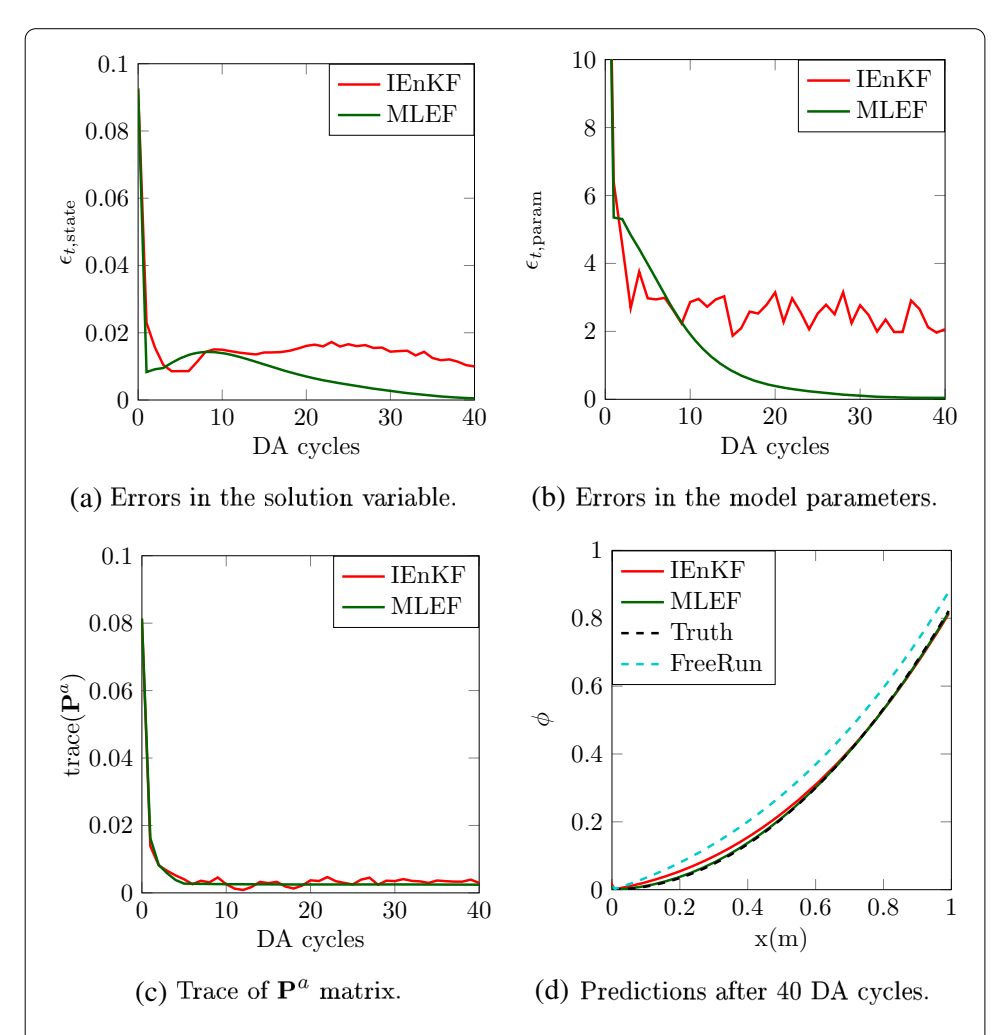


Fig. 6 Comparisons of various measures between the IEnKF (red line) and MLEF (green line) methods for the nonlinear test in case 2

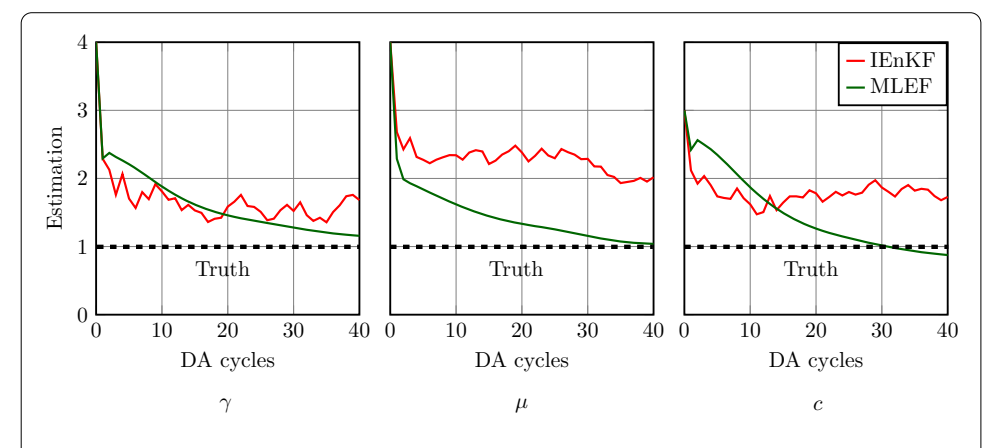


Fig. 7 The estimation of each model parameter in terms of ensemble mean $(\tilde{\gamma}, \tilde{\mu}, \text{ and } \tilde{c})$ by IEnKF (red line) and the control state $(\hat{\gamma}, \hat{\mu}, \text{ and } \hat{c})$ by MLEF (green line) for the nonlinear test in case 2

Table 4 The computational cost and the cost increment of each ensemble

Ensemble size	Total CPU cost (sec)	Increment (%)
4	0.563	
6	0.702	24.64
8	0.885	26.03
10	0.997	12.60
12	1.107	11.04
14	1.218	10.08

observation operator as defined in Eq. (36). The observations are still synthesized from the perfect model, but now they are at every other cell by adding noise with the error distribution N(0,0.75). The DA frequency and the time step size remain the same as those in the above case. The initial members are generated by the lagged forecast method with $t_{\tau}=250$. The summary of the DA+CFD configuration for the problem is recorded in Table 5. Figure 9 shows the spread of the members, the ensemble mean, and the truth. The results in Fig. 10 present the trajectory comparisons of both the observed element (X_5) and unobserved element (X_{16}) predictions along the entire DA process. The small black triangles indicate when the observations are available and assimilated into the DA+CFD system. By comparing the overall difference between the truth, the free CFD runs, and the predictions from the EnKF, IEnKF, and MLEF methods, all DA predictions are pulled toward the observation at the beginning of the DA process. However, only the MLEF prediction gets better converged toward the "truth" along the entire process. Partially, this may be due to the optimization at the analysis stage in the MLEF method.

We further assess the performance based on the measure of the RMS error. By tracking the trajectories of the convergence history of the RMS error over the DA cycles and comparing among the 3 different DA methods in Fig. 11a, we find that data assimilation is effective in the error reduction for the chaotic mode problem since all the RMS error values are reduced as more DA cycles are performed. Some fluctuations occur in the results by 3

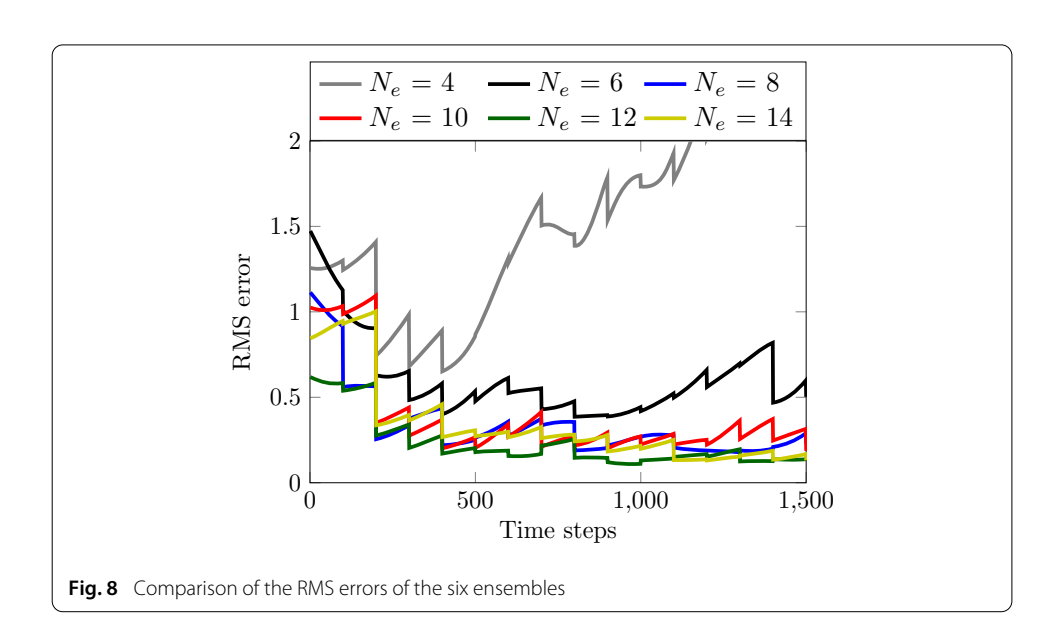


Table 5 DA+CFD configurations for imperfect initial condition in chaotic-mode problem (referred as "case 3")

Forward model	Configuration	
Equation	Lorenz 1996 model (see Sect. 4.2)	
Number of variables	20 (N = 20)	
Time step (Δt)	$\Delta t = 0.001 \mathrm{s}$	
Boundary condition	Inlet: Dirichlet boundary condition	
	Outlet: Neumann boundary condition	
DA	Configuration	
Size of the ensemble	12 (EnKF, IEnKF), 12 + 1 (MLEF)	
Uncertainty	Solution variable (X)	
Initial guess	X: generated by lagged forecast method	
Frequency	Linear test: 100 time steps	
	Nonlinear test: 200 time steps	
Synthesized observation	At every other cell:	
	Linear test: $\mathbf{O} = X$	
	Nonlinear test: $\mathbf{O} = 2.5X^2 + 1.5X$	
Methods	Linear test: EnKF, IEnKF, and MLEF	
	Nonlinear test: IEnKF and MLEF	
Total DA cycle	Linear test: 40 cycles	
	Nonlinear test: 20 cycles	

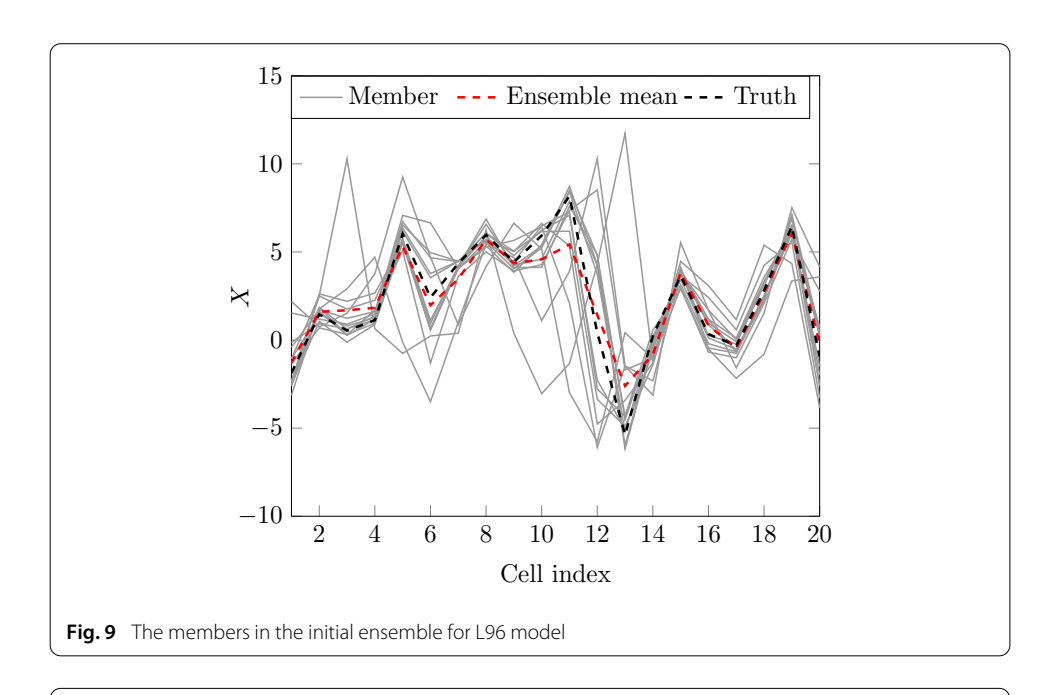
DA methods. But, the result of the MLEF method converges to a lower magnitude along the DA process. The final prediction by MLEF converges closer to the truth after 40 DA cycles in Fig. 11b, which shows that the MLEF has better convergence performance than the other two methods on addressing the chaotic dynamics.

More interestingly, we investigate the performance of the MLEF and IEnKF methods for the nonlinear quadratic observation operator, where $\mathcal{H}(\cdot)$ is given by

$$\mathcal{H}(X_j) = 2.5X_j^2 + 1.5X_j, \quad j = 1, 2, \dots, N_{\text{obs}}.$$
 (37)

Similarly, the observations are synthesized from the perfect model at every other cell by adding noise with the error distribution N(0, 0.25). In this case, because of the chaotic model problem and the nonlinearity introduced from the given observations, a very small perturbation in the DA initial conditions can lead to a significant deviation when testing both the IEnKF and MLEF methods. Instead, the observation error is reduced in order for us to focus on understanding the uncertainty reduction between the IEnKF and MLEF methods. The DA frequency is set to be every 200 time-steps, and the time step is still $\Delta t = 0.001$ s. The predictions of the observed element (X_5) and unobserved element (X_{16}) predictions are compared among the results of the IEnKF and MLEF, the truth, and the free CFD run in Fig. 12 along the entire DA process. The small black triangles still indicate when the observations are available and assimilated into the DA+CFD system. Clearly, both DA methods can result in pulling the forecasts to the truth, but the prediction by the MLEF method converges closer to the truth. Nevertheless, the predictions with DA converge toward the truth over the DA cycles, while the free CFD simulations are still apparently erroneous.

The assimilation performance is further investigated by tracking the RMS error over the DA cycles and comparing between the two DA methods. The trajectories of the conver-



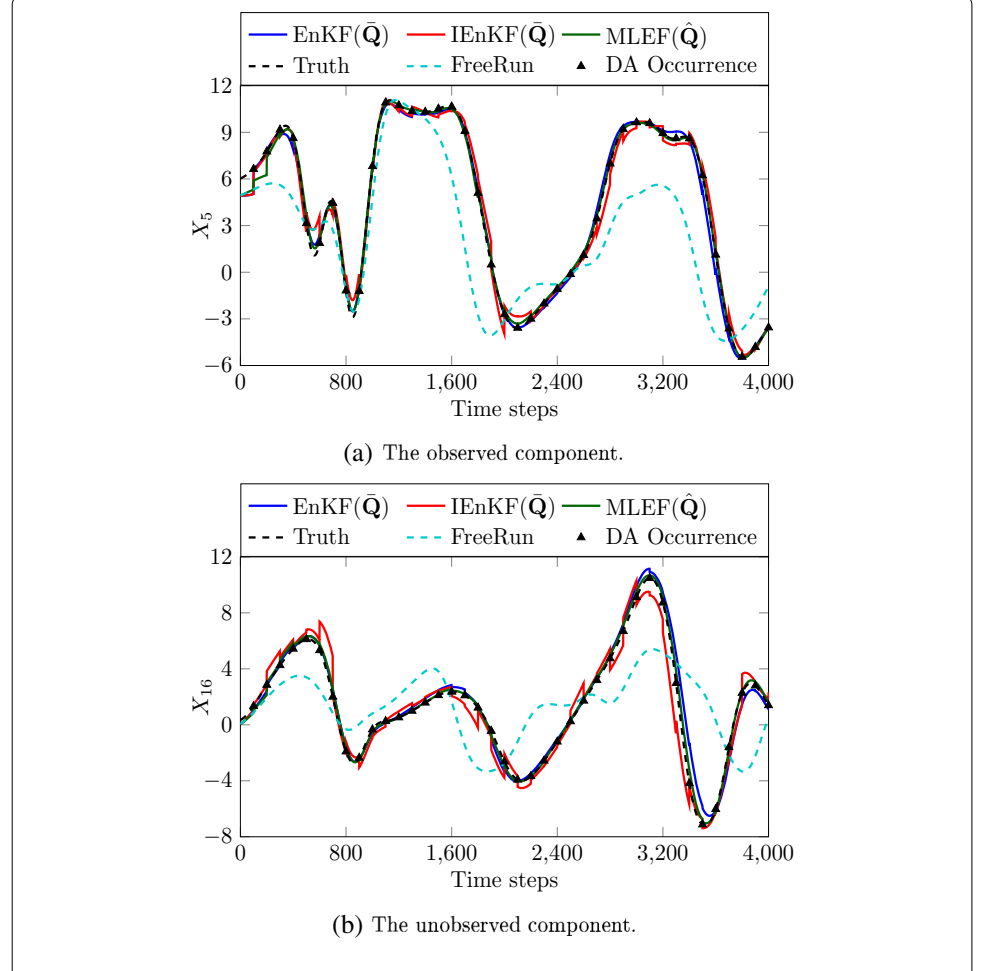


Fig. 10 Trajectory comparisons on the observed and unobserved components among the EnKF (blue line), IEnKF (red line), and MLEF (green line) methods for the linear test in case 3

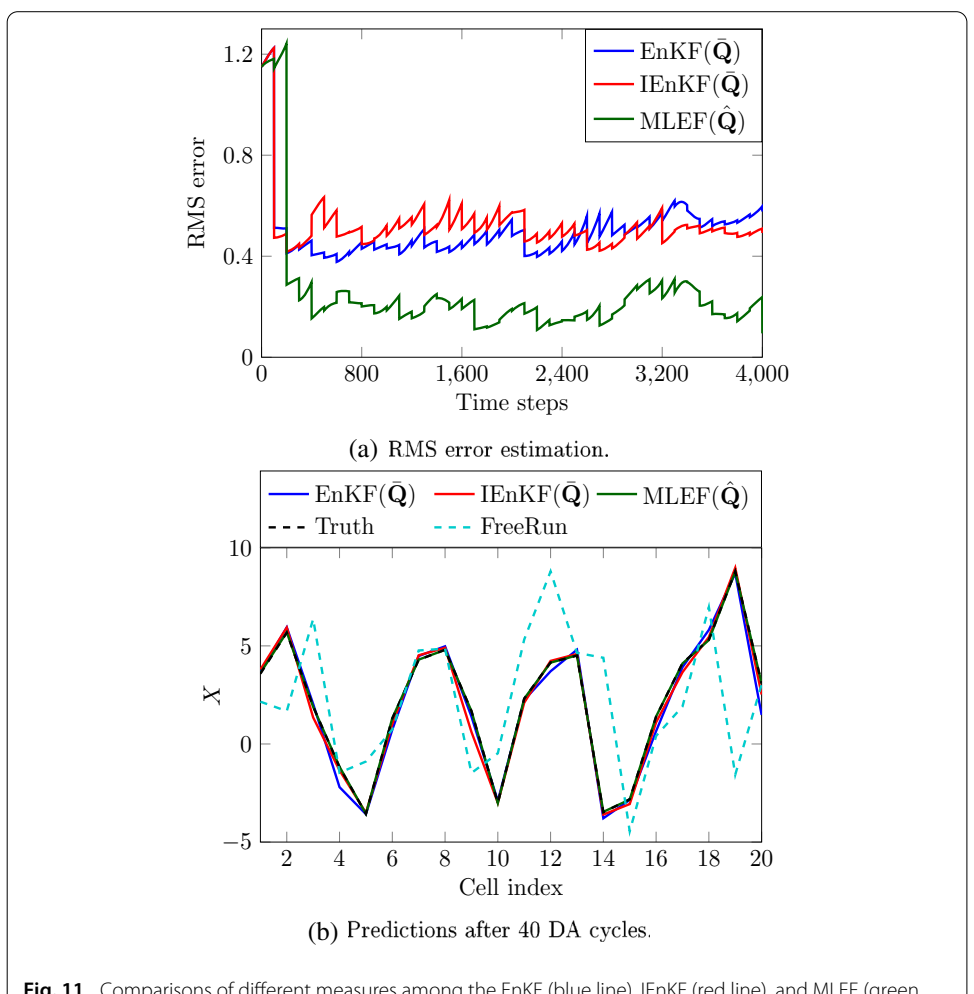


Fig. 11 Comparisons of different measures among the EnKF (blue line), IEnKF (red line), and MLEF (green line) methods for the linear test in case 3

gence history are plotted in Fig. 13a. They are clearly consistent with what we observed in Figs. 5c and 11a, which show that data assimilation is effective in the error reduction. The absolute solution difference is calculated and presented in Fig. 13b. The final prediction of MLEF shows a smaller difference than that in the prediction of the IEnKF, which can indicate that the MLEF method has better filter performance in addressing the nonlinearity of the observation operator than the IEnKF method does.

6 Conclusions and future work

The DA performance has been tested with two problems—one with a transient mode and the other with a chaotic nature. The first CDR problem involves three transient physical processes of convection, diffusion, and reaction (source), but the system eventually becomes steady. The second problem is the Lorenz 1996 chaotic model. The rationality of choosing the two-unit problems is based on that (i) both have the "truth" which can be used to assess the assimilation performance and predication accuracy easily, and (ii) complex engineering fluid dynamics problems are often characterized by physical processes involving convection, diffusion, and source, in addition to turbulence (chaos). On the observation operator, both the linear and nonlinear operators are studied. In engineering,

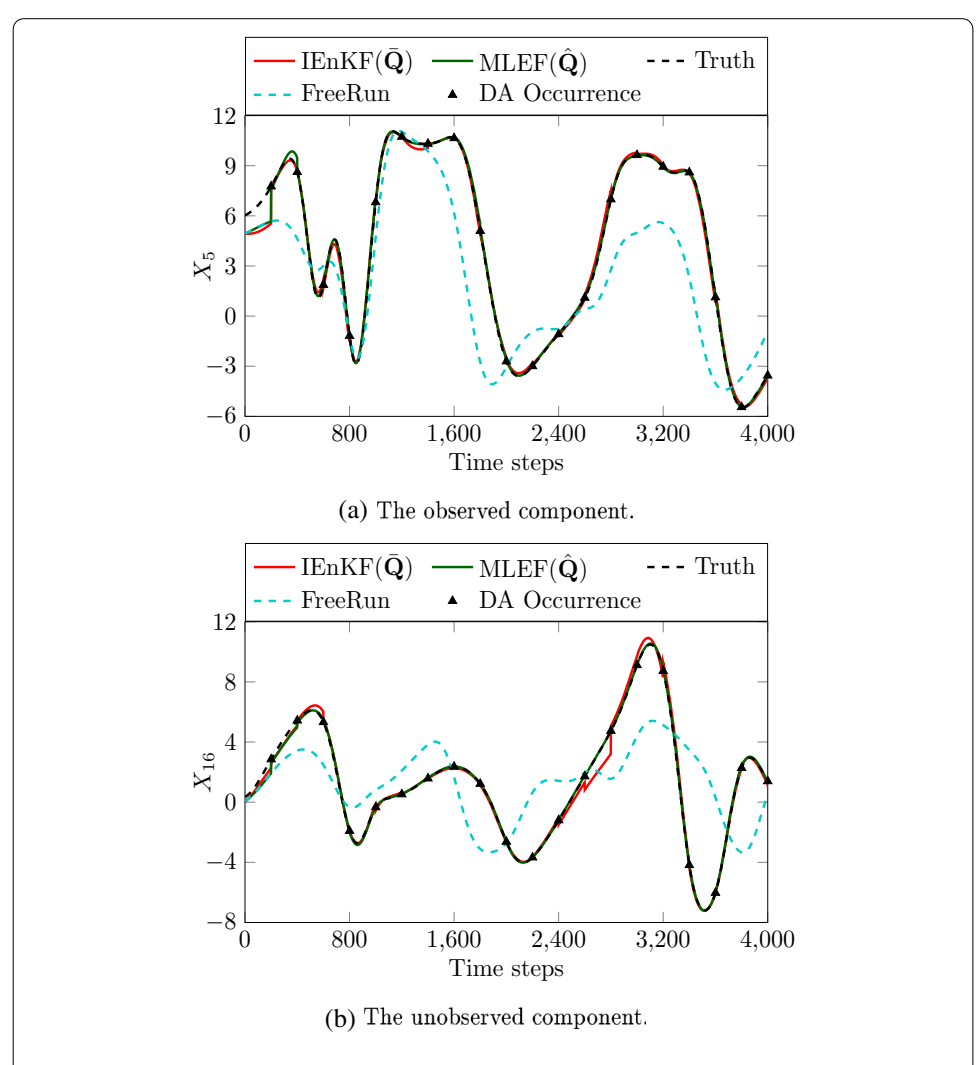


Fig. 12 Trajectory comparisons on the observed and the unobserved components between the IEnKF (red line) and MLEF (green line) methods for the nonlinear test in case 3

solution variables are not always observed, so nonlinear mapping between observation and state space is required. All DA methods are applied to demonstrate the reduction in the error of initial conditions, the improvement in the estimates of uncertain model parameters, and both simultaneously. Since the initial state and covariance are imperfect, we obtained that there is a time needed for data assimilation to reach its solution, typically after several DA cycles. To assess the performance of all three DA methods, the analysis ensemble means are plotted for the EnKF and IEnKF, while the deterministic analysis state is plotted for the MLEF method. Due to a large number of analyses, the ensemble mean of EnKF/IEnKF analyses may have a better chance to (accidentally) estimate analysis uncertainty in the beginning when all systems are trying to "learn" about the true state and its uncertainty. However, the "learning" process implied from the Bayes formula (i.e., Bayesian inference) appears to be more efficient in MLEF. Hence, the MLEF has theoretical advantages in producing more accurate solutions. It is possible that alternative choices of the initial state and uncertainty at the beginning of assimilation may produce less favorable conditions for EnKF/IEnKF during initial DA cycles, but this is out of the

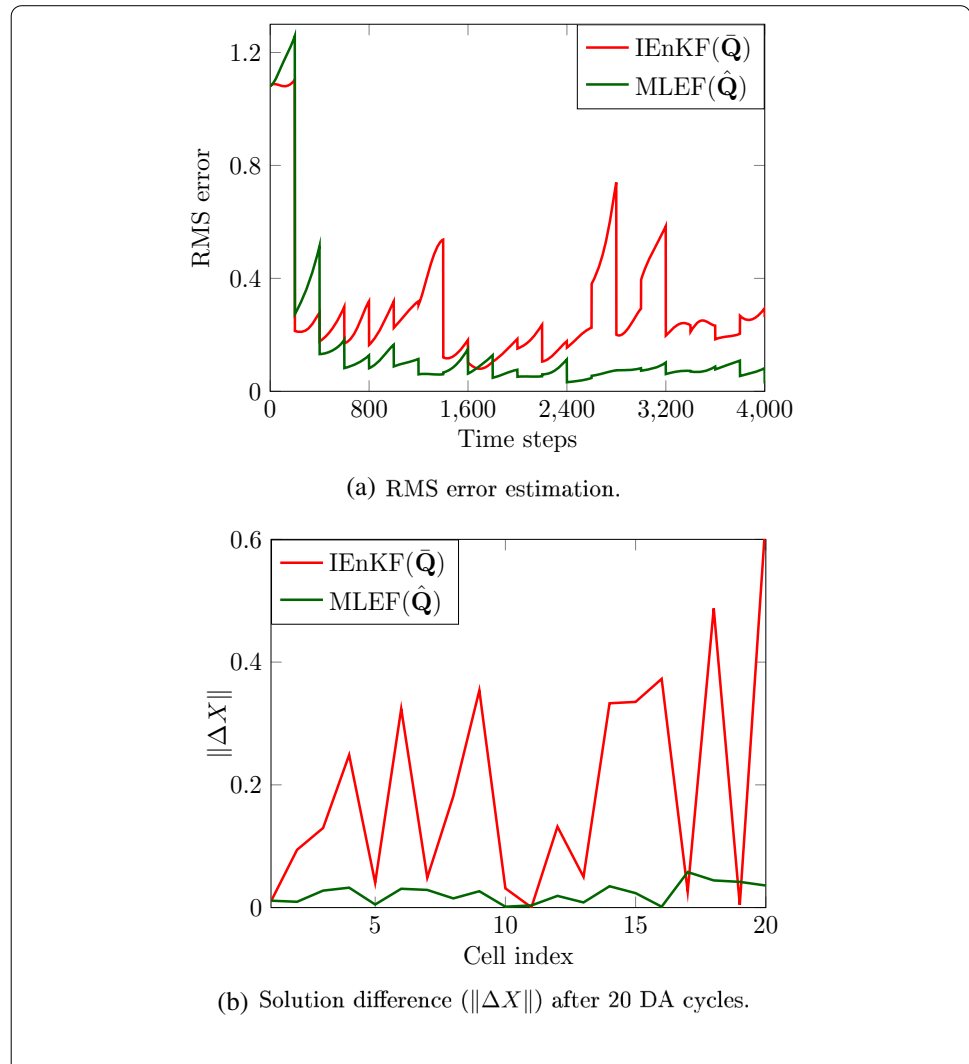


Fig. 13 Comparisons of different measures between the IEnKF (red line) and MLEF (green line) methods for the linear test in case 3

scope of this manuscript. Furthermore, based on the quality metrics (e.g., the true error, the trace of the error covariance matrix, and the root-mean-square error), the assessment of DA performance for the CDR problem shows that the MLEF method is superior to the EnKF method in both the computational efficiency and the solution accuracy in the case of the linear observation operator and the IEnKF method in the case of the nonlinear observation operator. Especially in the cases of the nonlinear observation operator, the MLEF demonstrates consistent efficiency and effectiveness in improving the estimates of the model parameters and predictions. The MLEF outperforms the EnKF in the linear observation operator case and the IEnKF in the nonlinear observation operator case for the chaotic dynamics. The excellent performance of the MLEF can be attributed to its mechanism in the forecast error covariance estimation, which is dynamically updated and consistently incorporates the information of the dynamical system. While any DA method will reduce uncertainty, the main challenge is not only to minimize uncertainty but also to estimate uncertainty that realistically corresponds to the optimal state obtained by minimization. That can be produced by the MLEF method for the time-dependent estimate of the uncertainty of the dynamical system. This information is essential for engineering applications.

For future work, we will demonstrate a new approach to address non-Gaussianity by integrating the MLEF with an implicit particle filtering method for further extending its application to study critical information on the flow laminar-to-turbulence transition process.

Funding

National Science Foundation (1723191 and 1723066).

Data availability

Data sharing is not applicable to this article as no real-world datasets were generated or analyzed during the current study. The synthesized datasets generated during and/or analyzed during the present study are available from the corresponding author on reasonable request.

Author details

¹Computational Fluid Dynamics and Propulsion Laboratory, Colorado State University, Fort Collins 80523, CO, USA, ²Cooperative Institution for Research in the Atmosphere, Colorado State University, Fort Collins 80523, CO, USA, ³Department of Mathematics, University of Kansas, Lawrence 66045, KS, USA.

Received: 17 December 2021 Accepted: 13 September 2022 Published online: 03 October 2022

References

- 1. Anderson, J.L.: An ensemble adjustment Kalman filter for data assimilation. Mon. Weather Rev. 129, 2884–2903 (2001)
- Bannister, R.N.: A review of operational methods of variational and ensemble-variational data assimilation. Q. J. R. Meteorol. Soc. 143, 607–633 (2017)
- 3. Bell, B.M.: The iterated Kalman smoother as a Gauss-Newton method. SIAM J. Optim. 4, 626-636 (1994)
- Bishop, C., Etherton, J., Majmudar, S.J.: Adaptive sampling with the ensemble transform Kalman filter. Part I: theoretical aspect. Mon. Weather Rev. 129, 420–430 (2001)
- Evensen, G.: The ensemble Kalman filter: theoretical formulation and practical implementation. Ocean Dyn. 53, 343–367 (2003)
- 6. Evensen, G.: Data Assimilation: The Ensemble Kalman Filter. Springer, Heidelberg (2007)
- Gao, X., Liu, J.: Data assimilation for computational fluid dynamics modeling of combustion. In: 26th International Conference on Parallel Computational Fluid Dynamics (2014)
- Gao, X., Wang, Y., Overton, N., May, I., Tu, X.: Estimation of flame speed model parameter using ensemble Kalman filter algorithm. In: Fall Meeting of the Western States Section of the Combustion Institute (2015). WSSCI 2015-134IE-0013
- 9. Gao, X., Wang, Y., Overton, N., May, I., Tu, X.: Data assimilated computational fluid dynamics algorithm for combustion. In: AIAA 2016-1810, 54th AIAA Aerospace Sciences Meeting (2016)
- Gao, X., Wang, Y., Overton, N., Zupanski, M., Tu, X.: Properties of a modified ensemble Kalman filter algorithm for combustion application. In: AIAA 2016-3484, 46th AIAA Fluid Dynamics Conference (2016)
- Gao, X., Wang, Y., Overton, N., Zupanski, M., Tu, X.: Data-assimilated computational fluid dynamics modeling of convection-diffusion-reaction problems. J. Comput. Sci. 21, 38–59 (2017)
- Haug, E.J., Arora, J.S., Matsui, K.: A steepest-descent method for optimization of mechanical systems. J. Optim. Theory Appl. 19, 401–424 (1976)
- Houtekamer, P.L., Mitchell, H.L.: A sequential ensemble Kalman filter for atmospheric data assimilation. Am. Meteorol. Soc. 129, 123–137 (2001)
- 14. Hurst, C., Gao, X.: Increasing the finite limit of predictability in turbulence by data assimilation. Technical report, AIAA Science & Technology 2020 Forum (2020)
- 15. Jazwinski, A.H.: Stochastic Processes and Filtering Theory. Academic Press, New York (1970)
- Kalnay, E.: Atmospheric Modeling, Data Assimilation and Predictabilty, 1st edn. Cambridge University Press, Cambridge (2003)
- 17. Kleist, D.T., Ide, K.: An OSSE-based evaluation of hybrid variational-ensemble data assimilation for the NCEP GFS. Part I: system description and 3d-hybrid results. Mon. Weather Rev. **143**, 433–451 (2015)
- Labahn, J., Wu, H., Coriton, B., Frnak, J., Ihme, M.: Data assimilation using high-speed measurement and LES to examine local extinction events in turbulent flames. Proc. Combust. Inst. 37, 2259–2266 (2019)
- Le Dimet, F.-X., Talagrand, O.: Variational algorithms for analysis and assimilation of meteorological observations: theoretical aspects. Tellus A 38A, 97–110 (1986)
- 20. Li, Z., Navon, I.M.: Optimality of variational data assimilation and its relationship with the Kalman filter and smoother. O. J. R. Meteorol. Soc. 127, 661–683 (2001)
- 21. Lorenz, A.C.: Analysis methods for numerical weather prediction. Q. J. R. Meteorol. Soc. 112, 1177–1194 (1986)
- 22. Lorentzen, R.J., Naevdal, G.: An iterative ensemble Kalman filter. IEEE Trans. Autom. Control **56**(8), 1990–1995 (2011)
- 23. Luenberger, D.L.: Linear and Non-linear Programming, 2nd edn. Addison-Wesley, Boston (1984)
- Navon, I.M., Wright, S.J.: Conjugate gradient methods for large-scale minimization in meteorology. Mon. Weather Rev. 115, 1479–1502 (1987)

- 25. Neave, H.R.: On using the box-muller transformation with multiplicative congruential pseudo-random number generators. J. Roy. Stat. Soc. Ser. C (Appl. Stat.) 21(1), 92–97 (1973)
- 26. Nocedal, J., Wright, S.J.: Numerical Optimization. Springer, Berlin (1999)
- 27. Parrish, D.F., Derber, J.C.: The national meteorological center's spectral statistical interpolation analysis system. Mon. Weather Rev. 120, 1747-1763 (1992)
- 28. Rabier, F., Jarvinen, H., Klinker, E., Simmons, A.J.: The ECMWF operational implementation of four-dimensional variational assimilation. I: experimental results with simplified physics, O. J. R. Meteorol, Soc. 126, 1143–1170 (2007)
- 29. Sakov, P., Oliver, D.S., Bertino, L.: An iterative EnKF for strongly nonlinear systems. Mon. Weather Rev. 140, 1988–2004
- 30. Suzuki, K., Zupanski, M.: Uncertainty in solid precipitation and snow depth prediction for Siberia using the Noah and Noah-MP land surface models. Front. Earth Sci. (2018). https://doi.org/10.1007/s11707-018-0691-2
- 31. Talagrand, O.: Assimilation of observations-an introduction. J. Meteorol. Soc. Jpn **75**, 191–209 (1997)
- 32. Talagrand, O., Courtier, P.: Variational assimilation of meteorological observations with the adjoint vorticity equation. I: Theory. J. Meteorol. Soc. 113, 1311-1328 (1987)
- 33. VanLeeuwen, P.J.: Particle filtering in geophysical system. Mon. Weather Rev. 2137, 4089–4114 (2009)
- 34. Wang, X.: Application of the WRF hybrid ETKF-3DVAR data assimilation system for hurricane track forecasts. Am. Meteorol, Soc. 26, 868-884 (2011)
- 35. Wang, Y., Gao, X.: Estimation of multiple model parameters using a data-assimilated CFD algorithm. In: Fall Meeting of the Western States Section of the Combustion Institute (2017). WSSCI 2017-29IT-0076
- 36. Wang, Y., Gao, X.: Covariance correction to the ensemble Kalman filter in a data-assimilated CFD algorithm for the convection-diffusion-reaction equation. In: AIAA 2017-3630, 23rd AIAA Computational Fluid Dynamics Conference (2017), https://doi.org/10.2514/6.2017-3630
- 37. Wang, X., Barker, D.M., Snyder, C., Hamill, T.M.: A hybrid ETKF-3DVAR data assimilation scheme for the WRF model. Part I: observation system simulation experiment. Mon. Weather Rev. 136, 5116-5131 (2008)
- 38. Wang, Y., Walters, S., Guzik, S., Gao, X.: CFD modeling of bluff-body stabilized premixed flames with data assimilation. In: AIAA 2020-0352, 2020 AIAA Science and Technology Forum (January 2020)
- 39. Wang, Y., Guzik, S., Zupanski, M., Gao, X.: The maximum likelihood ensemble filter for computational flame and fluid dynamics. IMA J. Appl. Math. 86(4), 631-661 (2021). https://doi.org/10.1093/imamat/hxab010
- 40. Whitaker, J.S., Hamill, T.M.: Ensemble data assimilation without perturbed observations. Mon. Weather Rev. 130, 1913-1924 (2002)
- 41. Xiao, H., Wu, J.-L., Wang, J.-X., Sun, R., Roy, C.J.: Quantifying and reducing model-form uncertainties in Reynoldsaveraged Navier-Stokes simulations: a data-driven, physics-informed Bayesian approach. J. Comput. Phys. 324,
- 42. Yang, S., Kalnay, E., Hunt, B.: Handling nonlinearity in an ensemble Kalman filter: experiments with the three-variable Lorenz model. Mon. Weather Rev. 140, 2628–2646 (2012)
- 43. Zupanski, M.: Regional four-dimensional variational data assimilation in a guasi-operational forecasting environment. Mon. Weather Rev. 121, 2396-2408 (1993)
- 44. Zupanski, M.: Maximum likelihood ensemble filter: theoretical aspects. Mon. Weather Rev. 133, 1710–1726 (2005)
- Zupanski, M., Navon, I.M., Zupanski, D.: The maximum likelihood ensemble filter as a non-differentiable minimization algorithm. Q. J. R. Meteorol. Soc. 113(D20110) (2008)

Publisher's Note

Springer Nature remains neutral with regard to jurisdictional claims in published maps and institutional affiliations.

Springer Nature or its licensor holds exclusive rights to this article under a publishing agreement with the author(s) or other rightsholder(s); author self-archiving of the accepted manuscript version of this article is solely governed by the terms of such publishing agreement and applicable law.